Chemical Geology

A new method for estimating parent rock trace element concentrations from zircon

James B. Chapman [a,*], George E. Gehrels [a], Mihai N. Ducea [a,b], Nicky Giesler [a], Alex Pullen [a]

[a] Department of Geosciences, University of Arizona, Tucson, AZ, United States
[b] Faculty of Geology and Geophysics, University of Bucharest, Bucharest, Romania

A B S T R A C T

Zircon/bulk rock REE partition coefficients from natural samples correlate with REE concentration in zircon. The correlation is the strongest for the LREE and diminishes with decreasing ionic radius. The relationship between partition coefficient and REE concentration in zircon can be modeled as a power law and the coefficient (α) and exponent (β) terms for each of the REE are empirically determined using new and previously published data. A series of independent tests show that using variable partition coefficients based on the reported α and β terms commonly results in more accurate estimates of bulk rock REE concentrations than average partition coefficients, particularly for the LREE that have previously been difficult to constrain. These results provide a way to account for highly variable REE concentrations in zircon, which may be controlled by numerous processes such as surface enrichment, complex substitution mechanisms, or accidental sampling of sub-microscopic inclusions. The proposed method for estimating bulk rock REE concentrations is especially well-suited to detrital zircon investigations where there is no information available on the parent rock composition.

© 2016 Elsevier B.V. All rights reserved.

1. Introduction

Zircon is the most commonly analyzed accessory mineral and is routinely employed in U–Th–Pb geochronology, U–Th/He and fission track thermochronology (Reiners, 2005), radiogenic (Hf) and stable (O) isotopic studies (Kinny and Maas, 2003; Valley et al., 1994), crystallization thermometry (Watson and Harrison, 2005), and trace element geochemistry (Belousova et al., 2002). Zircon is also resistant to weathering and alteration, which makes it an ideal mineral for detrital studies. A critical presumption in detrital mineral studies is that data obtained from zircon is a proxy for the parent igneous rock rather than the sedimentary host rock. This is demonstrably true for most types of analyses, however, relating trace element and rare earth element (REE) concentrations in zircon to bulk rock or melt concentrations has proven difficult (Hoskin and Ireland, 2000; Coogan and Hinton, 2006). The incentive to establish more accurate estimates of parental bulk rock concentrations using in-situ zircon measurements is significant as it would link zircon to a large body of whole rock geochemical literature with numerous possible applications including studies of provenance, crustal thickness, mineral exploration, crustal evolution, metamorphism, and petrogenesis (e.g. Belousova et al., 2002; Grimes et al., 2015; Profeta et al., 2015; Nardi et al., 2013; Wilde et al., 2001; Rubatto, 2002).

The primary obstacle in using zircon chemistry to determine trace element concentrations in the parent rock is that trace element partition coefficients ($D_{element}^{zircon/bulk\ rock}$) vary by up to several orders of magnitude, especially among the light rare earth elements (LREE) such as La (Hanchar and van Westrenen, 2007). There are many variables that affect partition coefficients including temperature, pressure, and oxidation state (Watson, 1985; Hoskin and Schaltegger, 2003; Rubatto and Hermann, 2007; Burnham and Berry, 2012; Trail et al., 2012; Taylor et al., 2015). Despite these variables, most researchers still use a single set of constant partition coefficients for relating zircon composition to bulk rock composition, which introduces significant uncertainty and inaccuracy into their conclusions. For example, Wilde et al. (2001) and Peck et al. (2001) converted trace element concentrations in Hadean zircons from the Jack Hills Quartzite into hypothetical bulk rock concentrations using the partition coefficients of Hinton and Upton (1991). They argued that the parental bulk rock was enriched in LREE and suggested that this might represent the earliest evidence of continental crust formation. However, these studies could have used other sets of partition coefficients (e.g. Bea et al., 1994) that would have indicated weak to no LREE enrichment in the parent rock. Several additional studies have highlighted the unreliability of zircon/bulk rock (or zircon/melt) partition coefficients and of REE concentrations in zircon themselves, emphasizing the need for a more comprehensive understanding of trace element partitioning in zircon (Whitehouse and Kamber, 2002; Cavosie et al., 2005; Hoskin, 2005; Coogan and Hinton, 2006; Trail et al., 2007; Harrison, 2009). While zircon/bulk rock partition coefficients, determined from natural studies, and zircon/melt partition coefficients,

* Corresponding author.
E-mail address: jaychapman@email.arizona.edu (J.B. Chapman).

determined from experimental studies, are similar for LREE, there are potential differences for HREE (Fig. 1). This study exclusively examines zircon/bulk rock partition coefficients.

REE partition coefficients between zircon and bulk rock can vary by several orders of magnitude, but the range of REE concentrations in crustal rocks is often relatively narrow, commonly less than two orders of magnitude (Fig. 2A). In contrast, there is relatively large variability in REE concentrations in zircon, even for carefully selected samples (Fig. 2B). This suggests that REE concentrations in zircon are disproportionately responsible for the range of partition coefficients. The relationship can be explored using a power law relating partition coefficient and REE concentration in zircon,

$$D_{REE}^{zr/br} = \frac{X_{REE}^{zr}}{X_{REE}^{br}} = \alpha \left(X_{REE}^{zr}\right)^{\beta} \tag{1}$$

where X_{REE}^{zr} and X_{REE}^{br} are the concentration of an individual REE in zircon and bulk rock respectively and α and β are theoretical variables. First, consider the classic scenario of constant partition coefficients that are independent of REE concentration in zircon (i.e. Henry's Law). In this scenario, REE concentration in zircon is linearly related to bulk rock REE concentration, which requires that $\beta = 0$ so that the partition coefficient $= \alpha$. Next, consider an opposite scenario where the REE concentration in zircon is completely independent of the bulk rock concentration. In this scenario, $\beta = 1$ and the bulk rock concentration $= \alpha^{-1}$. We envision a continuum between these two end-member scenarios such that $0 \leq \beta \leq 1$ for REE in zircon. When $0 < \beta < 1$ the concentration in zircon increases exponentially with increasing concentration in the parent rock. Larger β values are indicative of zircon REE enrichment (or depletion) processes besides equilibrium partitioning.

To estimate α and β, trace element concentrations in zircon were analyzed from a series of samples from the Coast Mountains Batholith of coastal British Columbia by laser ablation-inductively coupled plasma-mass spectroscopy (LA-ICP-MS). Zircon/bulk rock partition coefficients were calculated using previously published whole rock trace element data from the same samples (Girardi et al., 2012) (Table 1). The results were combined with partition coefficients from several previous studies that analyzed natural zircons with a large range of REE concentrations (Nagasawa, 1970; Fujimaki, 1986; Sano et al., 2002; Thomas et al.,
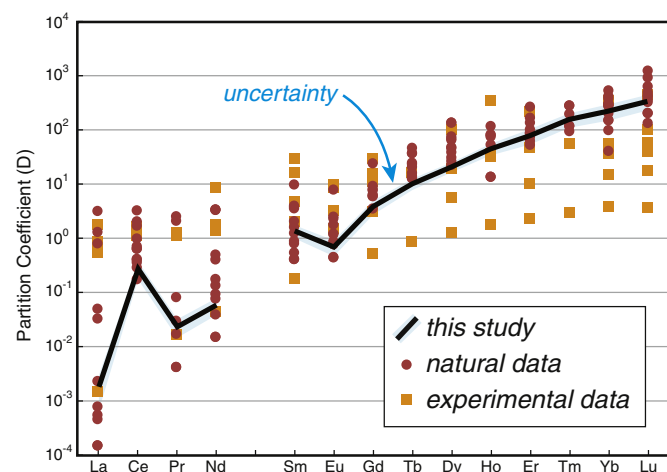

Fig. 2. A) Histograms of Yb and La concentrations (red bars) of ~40,000 plutonic and volcanic rocks from global convergent margins. Data is from the Geochemistry of Rocks of the Oceans and Continents (GEOROC; http://georoc.mpch-mainz.gwdg.de) database. Crustal abundances, plotted in blue, are from Rudnick and Fountain (1995). REE concentrations in crustal rocks commonly vary by <2 orders of magnitude. B) Histograms of Yb and La concentrations in individual zircons measured in this study after the removal of spurious data that may have been affected by the accidental sampling of inclusions (321 measurements), see text for details on the filtering method. Note that even after the careful selection of data, there is still large variability in zircon analyses. (For interpretation of the references to color in this figure legend, the reader is referred to the web version of this article.)

2002; Claiborne et al., 2010; Nardi et al., 2013) and fit with Eq. (1) to empirically determine α and β for each REE, Y, and Nb (Table 2, Fig. 3). Although not examined here, a similar method could potentially be applied to other trace elements in zircon (e.g. Sc, Ta). Eq. (1) can be applied as an alternate method for estimating bulk rock REE concentrations from in-situ measurements of zircon using the estimated values of α and β.

To illustrate the utility of this method, several examples from independent data sets are presented where bulk rock REE data and REE concentrations in zircon were acquired from the same sample. The bulk rock REE concentrations predicted by Eq. (1) can frequently approximate the measured bulk rock REE values and in some cases are more

Fig. 1. Previously published zircon/bulk rock (natural data; Nardi et al., 2013; Reid et al., 2011; Claiborne et al., 2010; Marshall et al., 2009; Sano et al., 2002; Thomas et al., 2002; Bea et al., 1994; Hinton and Upton, 1991; Fujimaki, 1986; Nagasawa, 1970) and zircon/melt (experimental data; Taylor et al., 2015; Burnham and Berry, 2012; Luo and Ayers, 2009; Rubatto and Hermann, 2007; Watson, 1980) partition coefficients. An identical plot with each data source separated by symbol and color is presented in Appendix 6 in the Supplementary Material. The zircon/bulk rock partition coefficient shown for this study is averaged from each of the median partition coefficients presented in Table 1 and the uncertainty is related to the scatter in those values (1σ).
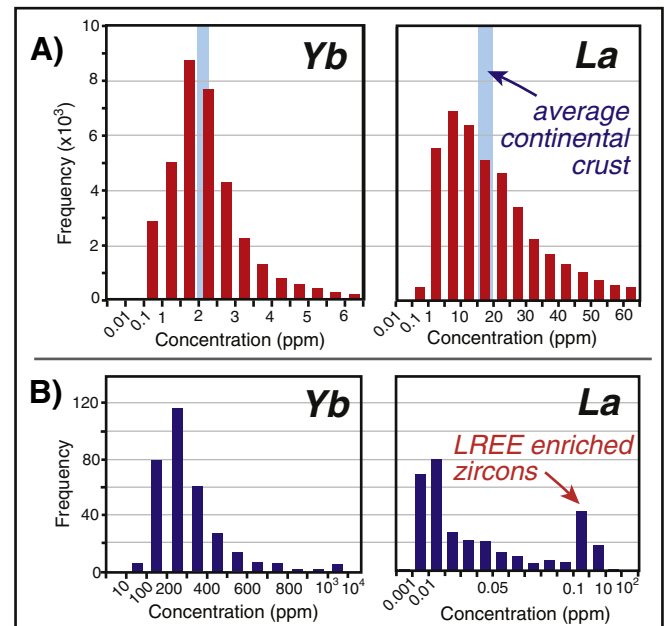
Table 1
Median zircon/bulk rock partition coefficients and median absolute deviation (MAD) calculated from the Coast Mountains Batholith samples analyzed in this study. The complete zircon data set is located in Appendix 3 in the Supplementary Material.

Element	Median $D^{zr/br}$	MAD
La	0.002	0.001
Ce	0.26	0.10
Pr	0.02	0.01
Nd	0.06	0.02
Sm	1.3	0.4
Eu	0.7	0.2
Gd	3.8	1.1
Tb	9.9	2.3
Dy	20	4
Y	47	10
Ho	44	11
Er	77	24
Tm	154	46
Yb	219	73
Lu	331	105
Nb	0.15	0.05

Table 2

Empirically determined α and β terms calculated by regressing Eq. (1) through plots of zircon/bulk rock partition coefficients vs. elemental concentration in zircon. The uncertainties reported for α and β include propagated errors associated with REE concentration for zircon measurements as well as errors associated with the regression. Ionic radii are reported in Å for 8-fold coordination (Shannon, 1976).

Element	α	±1σ	β	1σ	Ionic radius	Charge
La	0.035	0.004 0.003	0.945	0.029	1.16	3+
Ce	0.085	0.024 0.019	0.630	0.065	1.143	3+
Pr	0.147	0.018 0.016	0.889	0.045	1.126	3+
Nd	0.059	0.006 0.006	0.926	0.038	1.109	3+
Sm	0.431	0.091 0.075	0.824	0.076	1.079	3+
Eu	1.24	0.12 0.11	1.012	0.083	1.066	3+
Gd	0.484	0.179 0.131	0.858	0.092	1.053	3+
Tb	4.20	1.50 1.10	0.671	0.129	1.04	3+
Dy	3.93	3.14 1.75	0.542	0.122	1.027	3+
Y	2.41	9.16 1.91	0.487	0.221	1.019	3+
Ho	8.00	9.82 4.41	0.544	0.212	1.015	3+
Er	6.56	7.97 3.60	0.545	0.150	1.004	3+
Tm	25.18	26.96 13.02	0.534	0.192	0.994	3+
Yb	20.18	33.15 12.54	0.433	0.161	0.985	3+
Lu	53.05	68.26 29.85	0.434	0.187	0.977	3+
Nb	0.136	0.017 0.015	0.911	0.037	0.74	5+

accurate than using any constant set of partition coefficients. This is particularly true for the LREE, whose partition coefficients have historically been the most difficult to constrain or model (Hanchar and van Westrenen, 2007; Rubatto and Hermann, 2007).

2. Samples and methods

Zircon crystals were analyzed from 18 individual granitoid samples from the Coast Mountains batholith, a Mesozoic continental magmatic arc (Gehrels et al., 2009). The whole rock major and trace element composition of the samples was determined by X-ray fluorescence and solution ICP-MS respectively and is reported in Girardi et al. (2012). SiO_2 concentrations in the analyzed samples ranged from 51 to 76 wt.% (Table 3). Approximately 20 zircons were analyzed from each sample with a total of 359 analyses. Sample zircon crystals along with natural and synthetic reference materials were mounted in a 22 mm inner-diameter epoxied ring-form and sanded to expose the interior of the grains, identical to the procedures for the initial U–Pb investigation (Gehrels et al., 2008). Previous U–Pb analysis of this suite of zircon crystals showed limited inherited components or Pb loss (Gehrels et al., 2009). Given these observations and previous examination by optical and electron microscopy as well as cathodoluminescence (CL) imaging to identify inclusions, cracks, zoning, and metamict textures (Gehrels et al., 2009), ablation locations were selected using a combination of reflected light and CL imaging.

2.1. Instrumentation and analytical routine

Trace element data and U–Pb isotope ratios were collected at the Arizona LaserChron Center (laserchron.org) at the University of Arizona using a Teledyne Photon Machines G2™ solid state NeF excimer laser-

ablation (LA) system coupled to a Thermo Fisher Scientific ELEMENT 2 ™ single collector inductively coupled plasma mass spectrometer (ICP-MS). The output energy of the laser was fixed at 7 mJ and attenuated ~4% before ablation. The laser fluence was 7 J/cm². The 193 nm laser was operated at 480 bursts at 8 Hz for 60 s of ablation during the initial suite of analyses. Following method refinement, data were collected with a thyratron ArF excimer laser with 400 bursts at 7 Hz. All analyses were preceded by $n = 3$ pre-ablation "cleaning" laser bursts with a spot diameter of 50 μm. Analysis spot diameter was 40 μm with an estimated pit depth of ~20 μm based on a drill rate of 0.053 μm/pulse (Ibañez-Mejia et al., 2015). Samples were ablated in a rapid wash-out HeLex™ cell and the aerosolized analyte was extracted in a He carrier gas through Teflon-lined tubing to a 25 mL mixing bulb where it was mixed with Ar before introduction to the plasma torch. Cool, auxiliary, and sample gas flow were 16, 0.8, and 1.25 L/min, respectively.

A total of 30 masses were measured ranging from ^{29}Si to ^{238}U. Masses analyzed included the REE (-Pm) and masses for U–Pb age determinations (Gehrels et al., 2008). Specifically measured masses included ^{31}P, ^{49}Ti, ^{177}Hf, and ^{232}Th to help identify REE-rich titanite and phosphate (e.g. apatite, monazite) inclusions within zircon. Because P is usually present at lower concentrations than predicted by the xenotime substitution ($REE^{3+} + P^{5+} = Zr^{4+} + Si^{4+}$) (Reid et al., 2011), zircon analyses with P molar equivalents >0.1 REE + Y molar equivalents were discarded (27 analyses). Zircon analyses with Th > 1000 ppm (1 analysis) and Ti > 50 ppm (5 analyses) were also discarded. Element intensities during ablation were monitored for intensity spikes that may result from sampling inclusions. The P > REE + Y molar equivalents filter was able to isolate analyses with large P intensity spikes. A complete table of the measured masses is located in the supplementary material as Appendix 1. Intensities for ^{142}Nd were not corrected for the minor isobaric interference of ^{142}Ce. Future analyses will measure ^{146}Nd. The analytical routine uses both the magnetic and electric sector to separate and focus the ions and contained 7 magnet jumps. Magnet settling time was set at 0.25 s for the initial jump to the lowest measured mass (28.976 Da) and 21 ms for subsequent jumps to incrementally larger masses (Appendix 1). Within each magnet setting, post-electrostatic analyzer deflector voltages were automatically adjusted to change the mass arriving at the detector with 1 ms settling time between voltage changes.

Each individual analysis consists of an ~11 s gas baseline measurement with the laser off, ~60 s of ablation, and ~8 s of washout time for intensities to return to baseline levels after the laser stops firing. Each analysis contains a total of 73 scans, with 9 scans on backgrounds, 2 scans for signal ramp-up, 52 scans on peak intensities, and 10 scans on signal wash-out. Dwell time per isotope was initially adjusted based on count rates observed for the 91500 zircon reference material and further refined to optimize precision of elemental measurements. Dwell times ranged from 2 to 100 ms with 1 integration per peak per scan for the REE and 4 integrations per peak per scan for U, Th, Pb, and Hg isotopes (Appendix 1).

2.2. Data processing and standards

Elemental and isotopic abundances along with their uncertainties were calculated and fractionation corrected by analyzing reference materials interspersed between sample zircon crystals. U–Pb isotope ratio and trace element data was reduced separately. A complete table of U–Pb data and trace element data is located in the supplementary material as Appendices 2 and 3 respectively.

U–Pb isotopic data was reduced following Gehrels and Pecha (2014) and Ibañez-Mejia et al. (2015) with the in-house reduction program "AgeCalc." FC-1, SL, and R33 zircon reference materials were used to correct for isotope fraction and calculate systematic errors during U–Pb data reduction. FC is the primary standard (1098.8 ± 0.25 Ma; Hoaglund, 2010; Mattinson, 2010), SL (563.5 ± 3.2 Ma; Gehrels et al., 2008) and R33 (419.4 ± 1.3 Ma; Gehrels and Pecha, 2014) are the
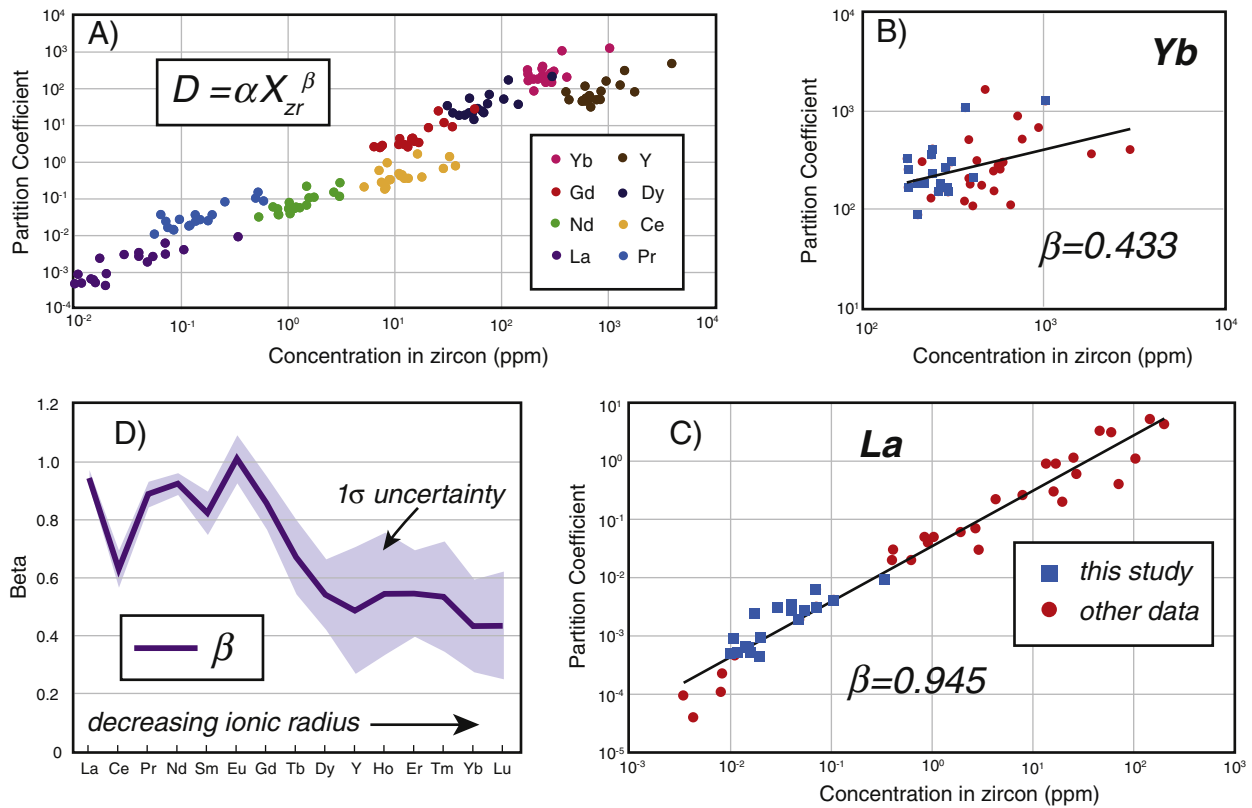
Fig. 3. A) Zircon/bulk rock partition coefficients for select REE calculated in this study from the Coast Mountains Batholith. There is a correlation between zircon concentration and partition coefficient that can be modeled by a power law relationship (Eq. (1)). The Coast Mountains Batholith data is combined with data from other studies to estimate α and β for the REE (Table 2). Examples of REE data fit with Eq. (1) to estimate α and β are shown for B) Yb and C) La. Other data sources include: Nardi et al. (2013), Sano et al. (2002), Fujimaki (1986), Nagasawa (1970), Claiborne et al. (2010), and Thomas et al. (2002). Identical plots of La and Yb with each data source separated by symbol and color is presented in Appendix 7 in the Supplementary Material. D) β is large for the LREE and decreases with decreasing ionic radius. The uncertainty associated with β increases for the HREE, which is related to the poor fit of the regression of Eq. (1) to the data as exemplified by Yb in part B of the figure.

secondary standards (all uncertainties are 2σ). The new U–Pb isotopic measurements and previously published data for these samples (Gehrels et al., 2009) overlap within error (generally <2%) for most samples (Appendix 2). One of the benefits of measuring U–Pb data and trace element data simultaneously is that the geochronology can help identify older inherited cores or complex zonation that may have different trace element concentrations. For example, in the study by Gehrels et al. (2009), sample 04GJP-09 contained older inherited cores, which were ~100 Ma older than domains along the rims of the crystals. As a test, this same sample was measured "blind" and 3 analyses were identified with older ages that were consistent with the inherited core ages. Despite the different U–Pb ages, the REE patterns were relatively similar, however, without the U–Pb age information it would not necessarily be obvious to treat this data separately. As always, it is important to carefully select analysis locations whenever possible.

Table 3

Data on each of the Coast Mountain Batholith samples including; bulk rock SiO$_2$ contents (weight %), median Ti concentrations in zircon (ppm), the median absolute deviation (MAD) of those Ti concentrations, zircon crystallization temperature estimated using the Ti-in-zircon thermometer of Ferry and Watson (2007) with α$_{TiO2}$ = 0.9 and α$_{SiO2}$ = 1, and propagated uncertainties for the crystallization temperature including errors associated with Ti measurements in zircon and uncertainties for the thermometer calculation (Ferry and Watson, 2007).

Sample	SiO$_2$ wt.%	Median Ti (ppm)	Ti MAD (ppm)	Temp (°C)	1σ (°C)
04GJP_43	51	18.8	0.9	785	40
04GJP_60	57.3	18.2	2.6	782	50
04GJP_62	58.8	5.4	0.4	671	36
04-GJP-01	57.5	11.8	1.2	740	42
04-GJP-09	66.4	7.2	2.2	696	57
04-GJP-16	72.7	3.5	0.9	638	47
04-GJP-22	63.1	3.8	0.8	644	45
04-GJP-23	75.9	6.1	2.3	681	62
04-GJP-24	63.5	12.4	1.6	745	46
04-GJP-29	54.5	4.2	0.8	653	43
04-GJP-32	71.4	5.8	1.7	678	55
04-GJP-37	59.7	15.0	2.5	763	50
04-GJP-39	70.9	13.0	2.2	749	50
04-GJP-40	65	4.8	0.7	662	41
MT05_102	59.2	11.7	1.8	739	48
MT05_106	63.2	5.0	1.2	665	49
MT05_98	68.9	9.2	1.4	717	46
MT05_99	62.2	18.9	1.5	785	44

Trace element data was reduced using the software program Iolite (Woodhead et al., 2007; Paton et al., 2010). Internal errors include uncertainties associated with background intensities, downhole fractionation, and scatter of measured intensities between repeat analyses of a sample. External errors include fractionation corrections for standards and uncertainty of standard concentrations. 91500 was used as the primary standard along with an internal Si standard to calculate all elemental concentrations except Ti, which is not reported for 91500 (Wiedenbeck et al., 2004). Ti data was reduced using NIST612 as the primary standard. 64 total measurements of Ti were made on 91500 with a concentration of 5.4 ± 0.5 ppm (1σ), which could potentially be used as a standard value. Appendix 4 in the supplementary material shows trace element concentrations of NIST612 calculated using 91500 as the primary standard.

3. Results

For each sample the median value of REE concentration in zircon was calculated from individual analyses of zircon from that sample and the median absolute deviation was calculated as a measure of uncertainty (Fig. 4A; Appendix 3). There is considerable variation in REE concentrations between zircons from the same sample (Fig. 4B) and the median absolute deviation of element concentration for each sample diverges by up to ~50% from the median. There is less median absolute deviation for the HREE and there is a weak to moderate positive correlation between median absolute deviation in concentration and wt.% SiO_2 in the bulk rock suggesting greater intra-sample variability in more felsic rocks (Appendix 5 in the supplementary material). There are several possible explanations for the wide range of REE concentrations in zircon and intra-sample variability including: mineral or melt inclusions (Hanchar and van Westrenen, 2007), fluid-modified zircon (Hoskin, 2005), complex substitution mechanisms (Finch et al., 2001), and disequilibrium partitioning related to zonation (Hofmann et al., 2009), sector domains (Reid et al., 2011; Chamberlain et al., 2013), boundary-layer effects (Watson and Liang, 1995; Watson, 1996; Hoskin, 2000), and a wide range of zircon crystallization temperatures (Hoskin and Schaltegger, 2003). These possibilities will be examined further in the discussion section below.

Calculated partition coefficients include propagated uncertainties for each sample using the median REE concentration in zircon and the bulk rock REE values from Girardi et al. (2012) (Table 1). The median partition coefficient from all of the samples in the Coast Mountains Batholith dataset are plotted in Fig. 1 against previously reported partition coefficients from natural and experimental studies.

3.1. Partition coefficients and element concentration

In Fig. 3A, several REE partition coefficients are plotted against median REE concentration in zircon from the Coast Mountains Batholith. For most elements, the positive correlation between partition coefficient and REE concentration in zircon can be modeled by the power law relationship in Eq. (1). To help constrain this relationship, the results are augmented with data from studies similar to this one that measured REE concentrations in natural bulk rock samples and in zircon extracted from the same bulk rock sample. The studies were chosen for the range of REE concentration in zircon and include concentrations determined by sensitive high resolution ion microprobe (SHRIMP) (Sano et al., 2002; Claiborne et al., 2010), laser-ablation ICP-MS (Nardi et al., 2013), and solution mass spectrometry (Nagasawa, 1970; Fujimaki, 1986). For the LREE, measurements by Thomas et al. (2002) were also included. Thomas et al. (2002) used secondary ion mass spectrometry (SIMS) to measure REE concentrations in zircon and in melt inclusions within zircon. Although the measurements by Thomas et al. (2002) are not strictly whole rock measurements, they were included for the LREE because they fill a data gap for moderately enriched zircons and the LREE partition coefficients from this study are considered reliable (Hanchar and van Westrenen, 2007).

For each REE, a least squares fit of Eq. (1) was used to estimate α and β (Table 2, Fig. 3B, C). As predicted, β for most REE is < 1 and > 0. Only Eu, whose concentration is affected by valence, early plagioclase crystallization, and oxidation state (Hoskin and Schaltegger, 2003; Trail et al., 2012) has $\beta > 1$. Overall, β is larger and α is smaller for the LREE compared the HREE (Fig. 3B–D). The uncertainty for β is the smallest for the LREE and increases for the HREE, consistent with a decrease in the influence of equilibrium partitioning (Fig. 3D). This relationship is perhaps not surprising considering that most crustal rocks are relatively enriched in LREE whereas zircon is LREE depleted (Bea et al., 1994). Even strong partitioning of LREE into zircon is unlikely to exert a significant influence on the bulk rock concentration, leading to β values closer to 1. Conversely, crustal rocks are relatively depleted in HREE and zircons are relatively enriched in HREE. Partitioning of HREE in zircon may have a more direct relationship to bulk rock concentration, with β values closer to 0.

In addition to the trivalent REE + Y, an estimate of α and β for Nb^{5+} is presented in Table 2. We expect a similar empirical relationship for other elements in 8-fold coordination (e.g. Ta^{5+}), but for many elements there is currently not enough data available at different concentration levels to make robust correlations (e.g. Sc).

3.2. Effect of temperature on partition coefficients

Previous experimental studies demonstrated that REE partition coefficients are dependent on crystallization temperature (Rubatto and Hermann, 2007; Burnham and Berry, 2012). These studies showed that for the HREE, increases in temperature result in a decrease in partition coefficient. The relationship between temperature and partition coefficients for the middle REE and LREE is less clear (Rubatto and
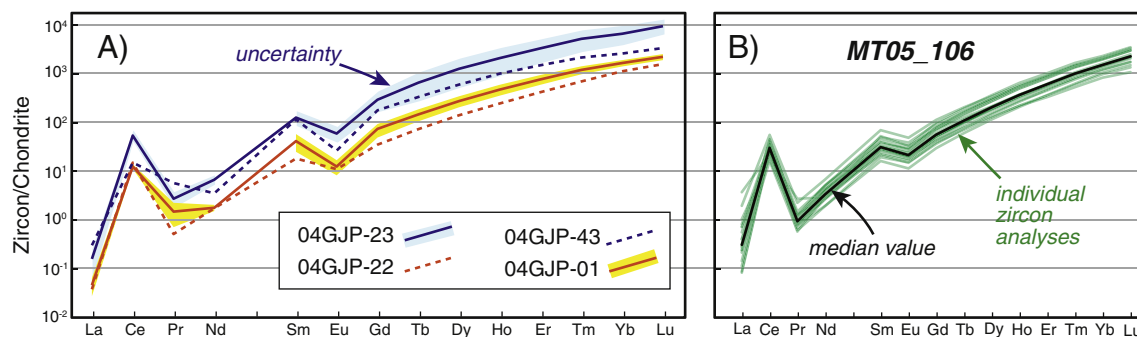

Fig. 4. A) plot of the median REE concentrations in zircon from four representative samples of the Coast Mountains Batholith data. For two of the samples, the median absolute deviation (uncertainty) is shown by the shaded area. These samples include the extremes in median concentrations. A full data table is presented in Appendix 3. B) plot of REE concentrations in individual zircons (20 total analyses) measured from sample MT05_106. Note the large range of La concentrations.
Chondrite normalization values are from McDonough and Sun (1995).

Hermann, 2007). Crystallization temperature for the Coast Mountain Batholith samples was calculated using the median Ti concentration in zircon for each sample using the method of Ferry and Watson (2007) (Table 3; Fig. 5). Major element analyses, abundant sphene, and common Ti oxides in the samples from the Coast Mountains Batholith (Girardi et al., 2012) suggest that rutile is at or close to saturation. The activation energy of TiO_2 (α_{TiO2}) was held constant at 0.9 and α_{SiO2} was held constant at 1. The results indicate that crystallization temperatures ranged from 638 to 785 °C for the Coast Mountains Batholith samples, with average errors of ~50 °C (Table 3; Fig. 5). Across the range of temperatures calculated, there is no clear correlation between temperature and partition coefficient (Fig. 5A). The results support previously proposed correlations for the HREE that include experimental and natural data representing a larger range of temperatures (Burnham and Berry, 2012) (Fig. 5B). While crystallization temperature may potentially help constrain partition coefficient estimates, its utility is currently limited to the HREE, which already have relatively well-constrained average partition coefficients (low β), and for zircon populations with a large range in crystallization temperatures.

4. Testing the empirical relationship

To test if Eq. (1) can be used to estimate zircon/bulk rock partition coefficients and ultimately to estimate bulk rock REE concentrations, a series of examples are presented in the following sections from studies that report bulk rock REE concentrations as well as REE concentrations in zircon derived from the same bulk rock sample. Based only on the REE concentrations in zircon, zircon/bulk rock REE partition coefficients are calculated using Eq. (1) and the values of α and β from Table 2. Next, bulk rock REE concentrations are estimated and compared against the measured bulk rock REE concentrations.

4.1. Intra-sample zircon variation

One of the problems in relating trace element concentrations in zircons to bulk rock concentrations is that there is significant scatter in the REE concentration in zircons from a single sample (Fig. 4B) (Chamberlain et al., 2013). Regardless of which partition coefficient is most appropriate, this suggests that for a given (constant) partition coefficient, many zircons from each parent rock need to be analyzed to average out intra-sample variation. For detrital studies, however, there is no way to know a priori which zircons should be grouped together so researchers have relied on techniques like grouping similar age populations together (e.g. Barth et al., 2013). In theory, using a variable

partition coefficient, as proposed by Eq. (1), may be able to reduce the need to average out intra-sample variation. The zircon/bulk rock partition coefficient estimate from with Eq. (1) changes along with changes in individual REE concentration in zircon.

To illustrate this possibility, bulk rock REE concentration estimates based on individual zircon analyses from a single sample using the median (constant) partition coefficients derived from the entire Coast Mountains Batholith dataset (Table 1) are plotted in Fig. 6A. Because these median partition coefficients come from only the Coast Mountains Batholith and include partition coefficients for the sample (04-GJP-39) shown in Fig. 6, they likely represent the most accurate possible set of (constant) partition coefficients available to use. However, even when using these "calibrated" partition coefficients, the range in estimated bulk rock REE concentrations are still prone to high errors for individual zircon analyses, particularly for the LREE (Fig. 6A). In contrast, using Eq. (1) with the values of α and β from Table 2 results in a more precise estimate of bulk rock REE concentrations (Fig. 6B) compared to constant partition coefficients (Fig. 6A).

4.2. Independent tests

In this section the accuracy of zircon/bulk rock partition coefficients estimated from Eq. (1) is tested with independent data sets (Fig. 7). In each data set examined, the median value of multiple individual analyses of REE in zircon is used along with median absolute deviation as a measure of uncertainty. This uncertainty is propagated into the calculation of bulk rock REE composition along with uncertainties related to α and β (Table 2). Uncertainty increases significantly for HREE estimates in accordance with the large uncertainties associated with α and β for the HREE (Fig. 3D). In addition to the estimate of bulk rock REE concentrations calculated from Eq. (1), estimates of bulk rock REE concentrations using the partition coefficients of Hinton and Upton (1991); Sano et al. (2002), and Nardi et al. (2013) are presented for each example. These partition coefficients are representative of the range of naturally determined partition coefficients (Fig. 1). The examples in Fig. 7 become increasingly complicated with samples that have more complex tectonic histories and varied geologic environments.

To start, Yang et al. (2011) present trace element data from a Permian andesitic tuff (sample TB065-1, $SiO_2 = 57$ wt.%) from central Tibet that was deposited in a continental arc setting (Fig. 7A). REE concentrations in zircon were measured by LA-ICP-MS and median absolute deviation is generally <50% of the median values. The partition coefficients of Sano et al. (2002) and those derived from Eq. (1) yield the closest approximations to the measured bulk rock concentrations (solution ICP-
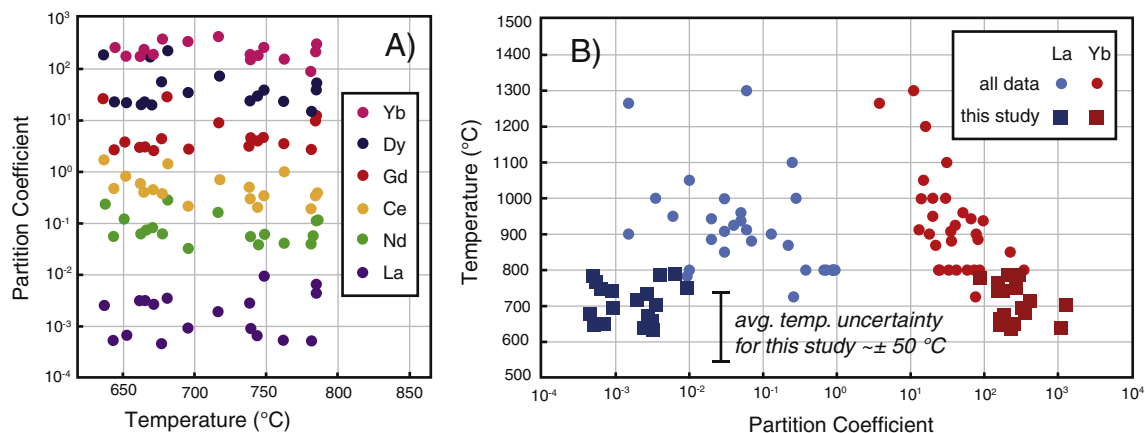

Fig. 5. A) Zircon/bulk rock partition coefficients determined for the Coast Mountains Batholith samples (Table 1) plotted against zircon crystallization temperature calculated using the Ti-in-zircon thermometer of Ferry and Watson (2007). There is no clear relationship between temperature and partition coefficient over the range of temperatures observed in the Coast Mountains data. B) Combining the Coast Mountains Batholith data with natural and experimental data on zircon partition coefficients over a larger range of temperatures (Thomas et al., 2002; Rubatto and Hermann, 2007; Luo and Ayers, 2009; Burnham and Berry, 2012) suggests that there may be a broader temperature dependence on partition coefficient. The temperature dependence is more well-defined for the HREE (e.g. Yb). The zircon crystallization temperature uncertainties for all samples analyzed in this study are ~±50 °C (Table 3).
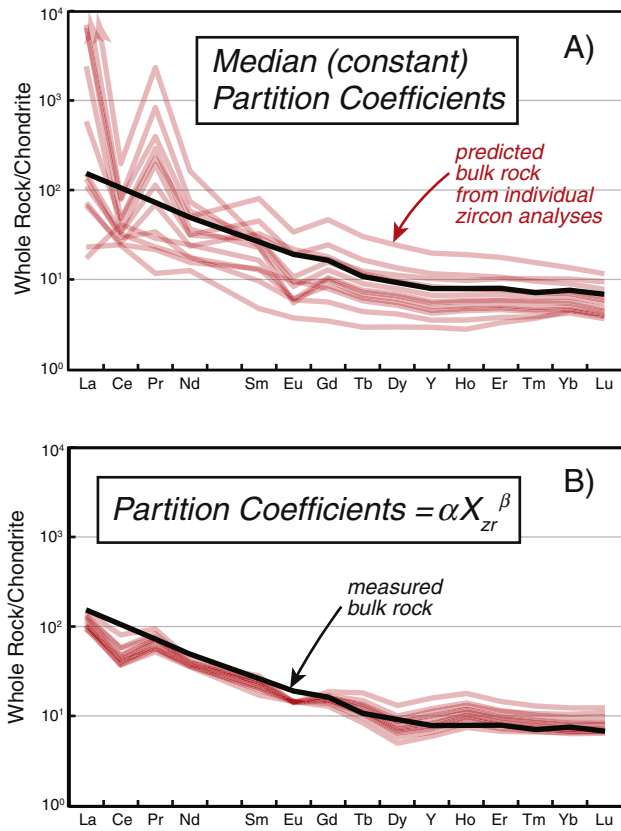
Fig. 6. Bulk rock REE concentration estimates for the Coast Mountains Batholith sample 04GJP-39 determined from individual zircon analyses using: A) median partition coefficients determined for the Coast Mountains Batholith (Table 1) and B) partition coefficients calculated with Eq. (1). Light red lines are predictions based on single zircon analyses and the thick black line is the actual (measured) bulk rock REE concentration. Uncertainties are not shown for each separate analysis, however, Fig. 7 shows representative uncertainties from estimated bulk rock REE concentrations. (For interpretation of the references to color in this figure legend, the reader is referred to the web version of this article.)

Chondrite normalization values are from McDonough and Sun (1995).

MS) (Fig. 7A). In the next example, Long et al. (2012) reported REE concentrations in zircon (LA-ICP-MS) from a Paleoproterozoic granite (sample T514; SiO_2 = ~76 wt.%) from the northern Tarim craton (Fig. 7B). The median absolute deviation is generally <60% of the median REE concentrations in zircon. In this case, the partition coefficients of Nardi et al. (2013) and those derived from Eq. (1) closely approximate the measured bulk rock concentrations (solution ICP-MS) (Fig. 7B). These paired examples (Fig. 7A and 7B) show that while a single set of constant partition coefficients may result in an accurate estimate of REE concentration in the bulk rock in a particular study, it cannot do so consistently across multiple studies. In contrast, using variable partition coefficients calculated from Eq. (1) can approximate bulk rock REE concentrations for both examples.

Fig. 7 illustrates that most partition coefficients, including partition coefficients estimated from Eq. (1), produce similar predictions of HREE concentrations in the parent rock. However, estimates of bulk rock LREE concentrations are much more variable and include large deviations from the measured values. Overestimation of the LREE in the parent rock is a common shortcoming of trace element studies of Hadean zircons (Whitehouse and Kamber, 2002; Coogan and Hinton, 2006; Cavosie et al., 2006). Whitehouse and Kamber (2002) present trace element zircon (ion microprobe) and bulk rock (solution ICP-MS) data from a relatively low-strain Archean gneiss in Greenland (sample SM/GR/98-2) (Fig. 7C). The median absolute deviation is generally <50% of the median REE concentrations in zircon. Whitehouse and Kamber (2002) show that the partition coefficients of Hinton and Upton

(1991), which were previously used to estimate bulk rock concentrations from Hadean zircons (Wilde et al., 2001, Peck et al., 2001), overestimate LREE in the Greenland gneiss. The partition coefficients derived from Eq. (1) can approximate the LREE concentrations in the bulk rock sample (Fig. 7C).

Fig. 7D presents an example from the Pleistocene Bishop Tuff in California. REE concentrations in zircon were measured by ion microprobe by Reid et al. (2011) and reported for both zircon rims and cores (samples 24-6, LV57, LV58, RPI). The median absolute deviation is generally <20% of the median REE concentrations in zircon rims and <30% in zircon cores. These samples are part of the early eruption phase of the Bishop Tuff recognized by Wilson and Hildreth (1997). REE concentrations of the bulk rock were estimated by Anderson et al. (2000) by analyzing melt inclusions in the same ignimbrite and ash fall layers that the zircon samples were extracted from. The median absolute deviation for REE concentrations in the melt inclusions is <15% of the median. Bulk rock estimates using the constant partition coefficients of Hinton and Upton (1991); Sano et al. (2002), and Nardi et al. (2013) are based on the REE concentrations in zircon rims. Bulk rock estimates using the partition coefficients from Eq. (1) produce similar results using either rim or core data (Fig. 7D). There is a pronounced Eu anomaly that is not well characterized by the partition coefficients calculated from Eq. (1), which further suggests that this method may be unreliable for Eu and Ce, which occur in multiple valence states and have more complex partitioning behavior (Trail et al., 2012).

The next two examples come from more complex geologic environments. Fig. 7E is a leucosome (sample NW10-36D; SiO_2 = 71 wt.%) in a migmatitic gneiss from an ultra-high pressure (UHP) terrane in Norway (Gordon et al., 2013). REE concentrations in zircon were determined by LA-ICP-MS and have large median absolute deviation of up to 90% of the median value. All of the partition coefficients (constant or variable method from Eq. (1) result in poor estimates of the REE concentrations in the parent leucosome (measured by solution ICP-MS) as well as the shape of the REE curve, showing a relative enrichment in HREE (Fig. 7E). These results indicate that metamorphic zircon and/or zircon from crustal melting in UHP terranes may pose problems for reproducing bulk rock concentrations.

Fig. 7F is a gabbro (sample JR31-22-1; SiO_2 = 51 wt.%) recovered from the Southwest Indian Ridge, an ultra-slow oceanic spreading center (Coogan et al., 2001). Bulk rock REE concentrations were determined by solution ICP-MS and REE concentrations in zircon were determined by SIMS (Grimes et al., 2007). The median absolute deviation of REE concentrations in zircon is generally <40% of the median. These zircons are a classic example of "oceanic zircon" that are known to have distinct trace element signatures (Grimes et al., 2015). In this example, the partition coefficients of Hinton and Upton (1991), originally calculated from a basanitic diatreme, most closely approximate the bulk rock REE composition whereas the partition coefficients calculated from Eq. (1) overestimate the bulk rock LREE concentrations. The results indicate that Eq. (1) may not be applicable to zircon derived from oceanic lithosphere.

In all of these examples, the partition coefficients derived from Eq. (1) do not result in perfect estimates of REE concentrations in the parent rock. Nonetheless, in the examples from igneous zircon associated with non-metamorphosed continental crust, they can provide approximations for REE concentration in the parent bulk rock that are more accurate than estimates from constant partition coefficients. This is particularly important for analyses where the provenance of the analyzed zircon is unknown or in question (e.g. detrital studies).

5. Discussion

These results suggest that no single set of fixed zircon/bulk rock partition coefficients can consistently provide accurate estimates on bulk rock REE concentrations from either a single sample or between samples from different geologic environments. The results also suggest that for most REE, concentration in zircon increases exponentially
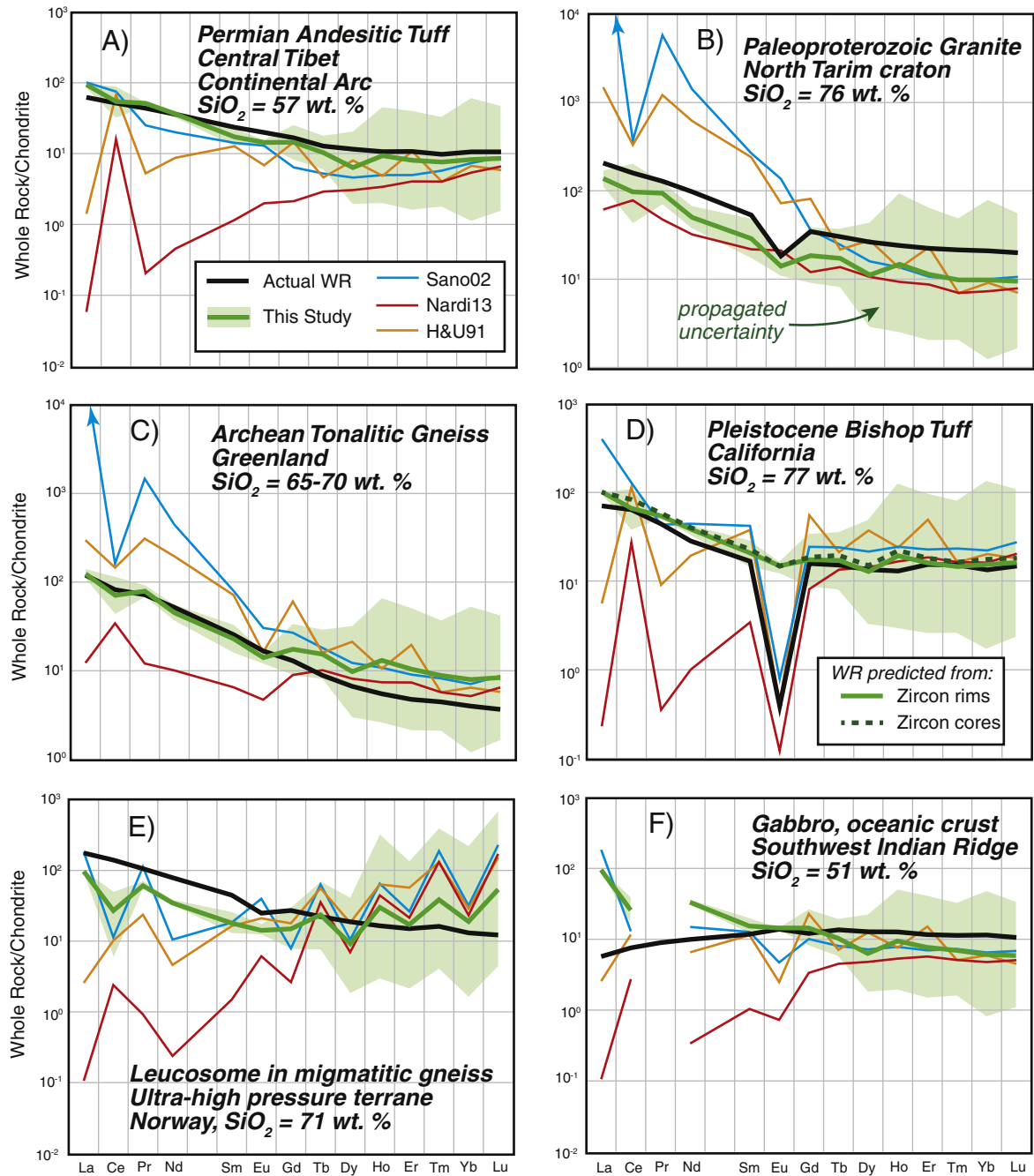
Fig. 7. Independent tests of bulk rock REE concentration predictions using Eq. (1) and the values of α and β presented in Table 2 (thick green line). For each example the median REE concentrations in zircon and median absolute deviation were calculated from individual zircon analyses of the same sample. Uncertainty associated these predictions includes errors in REE concentrations in zircon from the samples as well as errors related to α and β. The results of the bulk rock predictions from Eq. (1) are compared against bulk rock REE concentration prediction using constant partition coefficients (Sano02 = Sano et al., 2002; Nardi13 = Nardi et al., 2013; H&U91 = Hinton and Upton, 1991). The thick black line is the reported REE concentrations of the whole rock (WR) sample from which the zircons were extracted. A) Sample TB065-1 from Yang et al. (2011). B) Sample T514 from Long et al. (2012). C) Sample SM/GR/98/02 from Whitehouse and Kamber (2002). D) Zircon data from the early eruption phase of the Bishop Tuff (samples 24-6, LV57, LV58, RPI) that are separated by zircon rim and core analyses (Reid et al., 2011). The bulk rock REE composition comes from Anderson et al. (2000). E) Sample NW10-36D from Gordon et al. (2013). F) Sample JR31-22-1 with REE concentrations in zircon from Grimes et al. (2007) and bulk rock REE concentrations from Coogan et al. (2001). (For interpretation of the references to color in this figure legend, the reader is referred to the web version of this article.) Chondrite normalization values are from McDonough and Sun (1995).

with increases in the bulk rock concentration ($0 < \beta < 1$). A counterargument to this idea is that there are "true" constant zircon partition coefficients, but they are obscured by natural REE variability within zircon or systemic measurement errors. Below, this possibility is addressed at length, but ultimately we argue that the empirical observation indicating a relationship between REE concentration in zircon and partition coefficient is significant and may be useful tool to estimate bulk rock concentrations. A strength of the proposed method for estimating

zircon/bulk rock partition coefficients (and hence bulk rock concentrations) is that it can account for REE variation in zircon regardless of the exact mechanisms responsible for that variation.

5.1. Variable LREE enrichment in zircon

A common explanation for variation of REE in zircon is accidental sampling of REE bearing mineral inclusions, including monazite, apatite,

and titanite, which are all relatively enriched in LREE compared to zircon (Bea et al., 1994; Cavosie et al., 2006; Hanchar and van Westrenen, 2007). We are skeptical that inclusions are solely responsible for LREE variability. Careful selection of laser ablation spots by optical and electron microscopy and monitoring of P, Th, Ti, and Si intensities during ablation should be able to identify and filter out inclusions. If elevated concentrations of the mineral-forming elements (e.g. P) cannot be detected, it is unlikely that the trace element concentrations are large enough to significantly affect the zircon trace element concentrations. Still, it is possible that sub-microscopic inclusions are pervasive in natural zircon and could result in an overestimate of LREE partition coefficients (Hanchar and van Westrenen, 2007) or overestimate of bulk rock LREE concentration, depending on which zircon analyses were in error. In this case, the increase in β for the LREE (Fig. 3) could reflect studies that sampled variably LREE enriched zircon and Eq. (1) could help correct for this inadvertent sampling.

Elevated LREE concentrations in zircon may also be related to fluid-modified zircon or hydrothermal zircon that Hoskin (2005) proposed could be identified on (Sm/La)$_N$ vs. La plots. The Coast Mountains Batholith data generally plot outside of the hydrothermal zircon field, although there are several data points that could be considered hydrothermal (Fig. 8A). Ultimately, it is difficult to identify hydrothermal zircon by REE concentrations alone (Cavosie et al., 2006). Another possible mechanism for elevated LREE concentrations could be substitution into lattice defect sites related to U and Th decay (Whitehouse and Kamber, 2002). Following Whitehouse and Kamber (2002), (La/Gd)$_N$ vs. Th + U is plotted, where actinide concentration is a proxy for radiation induced lattice damage (Fig. 8B). LREE enrichment does not appear to correlate with lattice damage for the Coast Mountains Batholith data and in general it is unclear why the relatively large LREE would be preferentially incorporated into these sites over the other REE. In either scenario, the use of Eq. (1) could help to choose a partition coefficient more appropriate for LREE enriched zircon.

Another possible explanation for elevated LREE concentration in zircon is complex substitution mechanisms. Substitution of the trivalent REE is thought to occur primarily by the xenotime substitution, $REE^{3+} + P^{5+} = Zr^{4+} + Si^{4+}$ (Hoskin and Schaltegger, 2003). Because the ionic radii of the REE in 8-fold coordination (Table 2) are larger than ionic radius of 8-fold coordination Zr (0.84 Å), substitution into the Zr site introduces strain into the crystal lattice. This explains the greater incompatibility of the larger radius LREE compared to the HREE in zircon. Experimental studies have shown that with increasing REE concentration in the melt and increased REE substitution into zircon, the Si–O bond distance decreases and the Zr–O bond distance increases as the

lattice is strained (Hanchar et al., 2001). This suggests that REE may become more compatible in zircon with increasing REE concentration in the melt. LREE, which are too large to substitute in high concentrations, may disproportionately substitute into the lattice because the parental melt is enriched in LREE. Because the Si–O bond-distance decreases, eventually P cannot easily substitute for Si, which may limit REE substitution. Concentrations of P in most natural zircons and some experimental studies suggest that there is excess HREE in relation to P and that other charge balancing substitutions besides the xenotime substitution must be operating (Hanchar et al., 2001; Reid et al., 2011). Interestingly, these studies have also reported that P may be in excess of the LREE when considering the xenotime substitution (Finch et al., 2001; Hanchar et al., 2001). This may indicate that substitution of LREE are not P limited and may be influenced by other substitution mechanisms, perhaps related to REE concentration.

Variable REE concentrations in zircon may also be related to zonation or chemical domains. Chamberlain et al. (2013) showed that dark cathodoluminescent sectors contain molar equivalent REE + Y in excess of P whereas light cathodoluminescent sectors have REE + Y close to unity with P. These sector domains crystallized contemporaneously from the same melt suggesting that there was no difference in magmatic composition. Likewise, sub-micron scale zoning of REE concentration correlates with cathodoluminescent oscillatory banding within a single sector domain in zircon crystals (Hofmann et al., 2009). These observations have been linked to boundary layer effects and dynamics at the zircon/melt interface (Watson and Liang, 1995; Watson, 1996; Hoskin, 2000). Partitioning of REE between crystal and melt is related to the crystal growth rate and rate of diffusion, which can vary between different growth surfaces (Watson, 1996). Although in-situ analyses of REE in zircon can be carefully selected to avoid inner domains (e.g. inherited cores), sampling below the scale of zonation is generally not possible by LA-ICP-MS. In Fig. 7D, bulk rock REE concentrations were estimated using REE concentrations in both zircon rims and cores as reported in Reid et al. (2011). Because REE concentrations in zircon differed between the rim and core domains in this suite of samples, the partition coefficient calculated using Eq. (1) also differed. As a result, the bulk rock REE concentration prediction from both zircon rim and core analysis is similar.

Finally, REE variability in zircon may result from temporal changes in the magma composition. Zircon is ordinarily not the only REE-bearing phase in a bulk rock sample and it competes with these other phases (e.g. apatite, titanite) for the REE (Hoskin et al., 2000). Zircon has a relatively large range of crystallization temperatures and it is commonly found as inclusions in a range of other minerals or interstitial phases
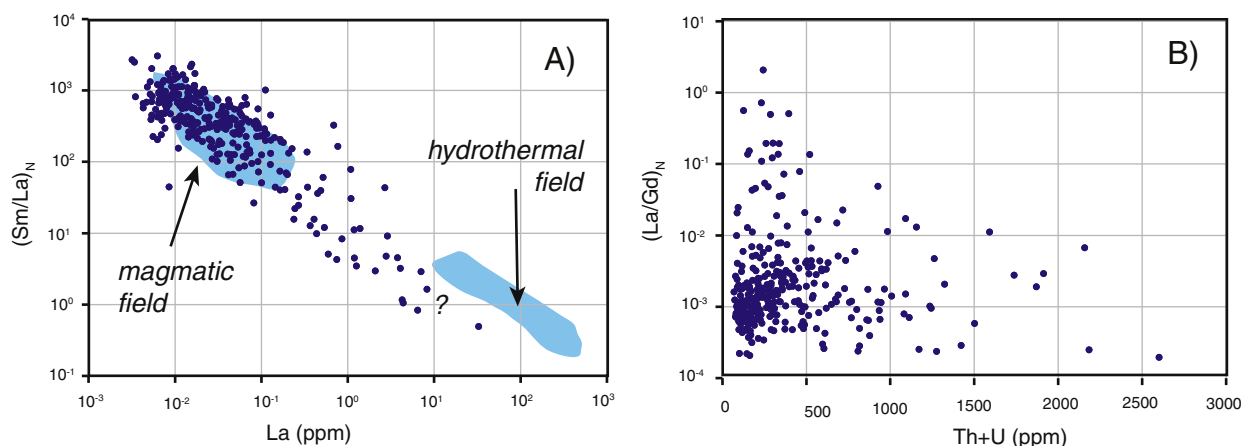

Fig. 8. A) Individual zircon analyses from the Coast Mountains Batholith data plotted on a (Sm/La)$_N$ vs. La discrimination diagram used by Hoskin (2005) to distinguish hydrothermal and magmatic zircon. Positively identifying hydrothermal zircon is difficult, but there may be several zircons affected by fluid interactions. B) Coast Mountains Batholith data plotted on a (La/Gd)$_N$ vs. Th + U diagram where actinide concentration is a proxy for radiation induced lattice damage (Whitehouse and Kamber, 2002). There is no evident increase in LREE fractionation with increasing Th + U.

suggesting a prolonged crystallization period (Watson and Harrison, 1983). As a result, REE concentrations in zircon may only represent the local REE environment (Hoskin and Schaltegger, 2003). Early crystallization of HREE-enriched (relative to the bulk rock) minerals like hornblende or late crystallization of zircon may result in LREE enrichment in zircon (Whitehouse and Kamber, 2002). It is possible that zircons from the same bulk rock sample record different magmatic compositions. Variable partition coefficient estimates from Eq. (1) may help to mitigate the effects that variable REE concentrations in zircon have on bulk rock REE concentration estimates.

5.2. Comparison to lattice strain model

Partition coefficients for REE in zircon can be approximated by lattice strain modeling based on the elastic properties of the Zr^{4+} substitution site (Blundy and Wood, 1994, 2003). A complication to lattice strain modeling is that experimental and naturally determined LREE partition coefficients are commonly larger than predicted (Hanchar and van Westrenen, 2007). Under the assumption that the larger-than-expected LREE partition coefficients are in error as a result of inclusions or melt composition uncertainty, LREE partition coefficients can be "corrected" by fitting lattice strain models to the HREE and middle REE partition coefficients (Hanchar and van Westrenen, 2007; Draper and van Westrenen, 2007; Taylor et al., 2015). There are several difficulties in using lattice strain modeling to determine appropriate partition coefficients. First, for single zircon analyses there is no constraint on which HREE partition coefficients to begin modeling with. Second, lattice strain modeling can provide acceptable fits to different sets of partition coefficients. For example, Hanchar and van Westrenen (2007) show that the partition coefficients of Sano et al. (2002) and Thomas et al. (2002) are both well-approximated by lattice strain modeling, however, the REE zircon/bulk rock partition coefficients from these studies vary by more than an order of magnitude, even though the errors associated with the studies are of the same magnitude or less than the reported partition coefficients. It is not clear which set of partition coefficients may be more appropriate to use. Third, for many sets of partition coefficients, lattice strain modeling suggests very small LREE partition coefficients. In some examples presented in Fig. 7, the partition coefficients of Hinton and Upton (1991) already overestimate LREE concentrations. Fitting the LREE partition coefficients of Hinton and Upton (1991) to a lattice strain model will result in even larger bulk rock concentration overestimates.

5.3. Improvements to method

Irrespective of the processes that lead to variable REE concentrations in zircon, the empirically determined values for α and β in Eq. (1) can help constrain which partition coefficient may be most appropriate and lead to more consistently accurate estimates of bulk rock concentrations. However, there are some inherent weaknesses to this method. First, although α and β were estimated from partition coefficients calculated from bulk rock analyses with a range SiO_2 contents (51 to 77 wt.%) and crystallization temperatures (650 to 900 °C), these analyses skewed toward intermediate to felsic compositions and moderate crystallization temperatures. The example presented in Fig. 7F shows that this method may not be applicable for zircon from very mafic parent rocks, including oceanic lithosphere (e.g. Grimes et al., 2007). When β = 1, α is constant, and the bulk rock concentration is independent of REE concentration in zircon. For the LREE, with large β (Table 2), the determination of α is accordingly critical. α^{-1} was empirically determined to be 28.6 for La, which is similar to the average abundance of La in the continental crust (18–30 ppm) (Rudnick and Fountain, 1995; Wedepohl, 1995) (Fig. 2). This suggests that this value of α is broadly appropriate for rocks associated with the continental crust, but highlights the limitations of this method for studying zircon from oceanic crust that has low average LREE abundances (e.g. La < 10 ppm;

Arevalo and McDonough, 2010). With prior knowledge about a geologic province, we speculate that refinements to α and β could be made that could improve bulk rock concentration estimates.

Another weakness of this method is that the correlation between REE concentration in zircon and partition coefficient is weak to poor for the HREE, resulting in large uncertainties (Table 2). Fortunately, β is small for the HREE and there is little change in the estimated partition coefficients with changes in REE concentration in zircon, but it is still uncertain if the bulk rock REE concentration predictions from Eq. (1) are any better than average partition coefficients from other studies, which already show relatively little variation for the HREE. If there is an underlying, systematic physical process responsible for variation in REE in zircon concentrations (e.g. substitution mechanisms) as opposed to a semi-random process (e.g. inclusions), then the observed decrease in β with decreasing ionic radii (Fig. 3D) may be reflective of this processes and application of Eq. (1) is appropriate for all REE, even when β is small.

6. Conclusions

New zircon trace element data and zircon/bulk rock partition coefficients are presented for granitoid samples from the Coast Mountains Batholith and combined with data from other studies that also present natural zircon/bulk rock partition coefficients. These data indicate that REE partition coefficients are positively correlated with REE concentration in zircon over several orders of magnitude. This relationship can be modeled using a power law relationship (Eq. (1)) and the empirically determined coefficient α and exponent β for the REE (Table 2). Using the proposed values for α and β, Eq. (1) yields estimates of bulk rock REE concentrations and REE patterns that in some cases are more accurate than bulk rock REE concentrations estimated from constant partition coefficients alone, particularly for the LREE (Fig. 7). A series of independent tests of this method for estimating bulk rock REE concentrations show that it may be broadly applicable to igneous zircon associated with the continental crust (e.g. continental arc magmatism).

Variable REE enrichment in zircon is likely the primary cause of the large range of naturally determined zircon/bulk rock partition coefficients. Although the method proposed here for estimating bulk rock REE concentrations from REE concentrations in zircon cannot distinguish between the many possible mechanisms for REE enrichment in zircon, it nonetheless appears to encompass the variation in constant zircon/bulk partition coefficients observed across multiple studies and may be a useful new tool to estimate bulk rock REE concentrations. This method may be most applicable for detrital zircon investigations when there is no constraint on which set of partition coefficients to apply.

Supplementary data to this article can be found online at http://dx.doi.org/10.1016/j.chemgeo.2016.06.014.

References

Anderson, A.T., Davis, A.M., Lu, F., 2000. Evolution of Bishop Tuff rhyolitic magma based on melt and magnetite inclusions and zoned phenocrysts. J. Petrol. 41, 449–473.
Arevalo, R., McDonough, W.F., 2010. Chemical variations and regional diversity observed in MORB. Chem. Geol. 271, 70–85.
Barth, A.P., Wooden, J.L., Jacobson, C.E., Economos, R.C., 2013. Detrital zircon as a proxy for tracking the magmatic arc system: the California arc example. Geology 41, 223–226.
Bea, F., Pereira, M.D., Stroh, A., 1994. Mineral/leucosome trace-element partitioning in a peraluminous migmatite (a laser ablation-ICP-MS study). Chem. Geol. 117, 291–312.

Belousova, E.A., Griffin, W.L., O'Reilly, S.Y., Fisher, N.J., 2002. Igneous zircon: trace element composition as an indicator of source rock type. Contrib. Mineral. Petrol. 143, 602–622.

Blundy, J.D., Wood, B.J., 1994. Prediction of crystal-melt partition coefficients from elastic moduli. Nature 372, 452–454.

Blundy, J.D., Wood, B.J., 2003. Partitioning of trace elements between crystals and melts. Earth Plan. Sci. Lett. 210, 383–397.

Burnham, A.D., Berry, A.J., 2012. An experimental study of trace element partitioning between zircon and melt as a function of oxygen fugacity. Geochim. Cosmochim. Acta 95, 196–212.

Cavosie, A.J., Valley, J.W., Wilde, S.A., 2005. Magmatic $\delta^{18}O$ in 4400–3900 Ma detrital zircons: a record of the alteration and recycling of crust in the Early Archean. Earth Plan. Sci. Lett. 235, 663–681.

Cavosie, A.J., Valley, J.W., Wilde, S.A., 2006. Correlated microanalysis of zircon: trace element, $\delta^{18}O$, and U–Th–Pb isotopic constraints on the igneous origin of complex >3900 Ma detrital grains. Geochim. Cosmochim. Acta 70, 5601–5616.

Chamberlain, K.J., Wilson, C.J.N., Wooden, J.L., Charlier, B.L.A., Ireland, T.R., 2013. New perspectives on the Bishop Tuff from zircon textures, ages and trace elements. J. Petrol. 55, 395–426.

Claiborne, L.L., Miller, C.F., Wooden, J.L., 2010. Trace element composition of igneous zircon: a thermal and compositional record of the accumulation and evolution of a large silicic batholith, Spirit Mountain, Nevada. Contrib. Mineral. Petrol. 160, 511–531.

Coogan, L.A., Hinton, R.W., 2006. Do the trace element compositions of detrital zircons require Hadean continental crust? Geology 34, 633–636.

Coogan, L.A., MacLeod, C.J., Dick, H.J.B., Edwards, S.J., Kvassnes, A., Natland, J.H., Robinson, P.T., Thompson, G., O'Hara, M.J., 2001. Whole-rock geochemistry of gabbros from the Southwest Indian Ridge: constraints on geochemical fractionations between the upper and lower oceanic crust and magma chamber processes at (very) slow-spreading ridges. Chem. Geol. 178, 1–22.

Draper, D.S., van Westrenen, W., 2007. Quantifying garnet melt trace element partitioning using lattice-strain theory: assessment of statistically significant controls and a new predictive model. Contrib. Mineral. Petrol. 154, 731–746.

Ferry, J.M., Watson, E.B., 2007. New thermodynamic models and revised calibrations for the Ti-in-zircon and Zr-in-rutile thermometers. Contrib. Mineral. Petrol. 154, 429–437.

Finch, R.J., Hanchar, J.M., Hoskin, P.W., Burns, P.C., 2001. Rare-earth elements in synthetic zircon: part 2. A single-crystal X-ray study of xenotime substitution. Am. Mineral. 86, 681–689.

Fujimaki, H., 1986. Partition coefficients of Hf, Zr, and REE between zircon, apatite, and liquid. Contrib. Mineral. Petrol. 94, 42–45.

Gehrels, G., Pecha, M., 2014. Detrital zircon U–Pb geochronology and Hf isotope geochemistry of Paleozoic and Triassic passive margin strata of western North America. Geosphere 10, 49–65.

Gehrels, G., Rusmore, M., Woodsworth, G., Crawford, M., Andronicos, C., et al., 2009. U–Th–Pb geochronology of the Coast Mountains batholith in north-coastal British Columbia: constraints on age and tectonic evolution. Geol. Soc. Am. Bull. 121, 1341–1361.

Gehrels, G.E., Valencia, V.A., Ruiz, J., 2008. Enhanced precision, accuracy, efficiency, and spatial resolution of U–Pb ages by laser ablation-multicollector-inductively coupled plasma-mass spectrometry. Geochem. Geophys. Geosyst. 9.

Girardi, J.D., Patchett, P.J., Ducea, M.N., Gehrels, G.E., Cecil, M.R., Rusmore, M.E., Wetmore, P., 2012. Elemental and isotopic evidence for granitoid genesis from deep-seated sources in the Coast Mountains Batholith, British Columbia. J. Petrol. 53, 1505–1536.

Gordon, S.M., Whitney, D.L., Teyssier, C., Fossen, H., 2013. U–Pb dates and trace-element geochemistry of zircon from migmatite, Western Gneiss Region, Norway: significance for history of partial melting in continental subduction. Lithos 170, 35–53.

Grimes, C.B., John, B.E., Kelemen, P.B., Mazdab, F.K., Wooden, J.L., Cheadle, M.J., Hanghøj, K., Schwartz, J.J., 2007. Trace element chemistry of zircons from oceanic crust: a method for distinguishing detrital zircon provenance. Geology 35, 643–646.

Grimes, C.B., Wooden, J.L., Cheadle, M.J., John, B.E., 2015. "Fingerprinting" tectono-magmatic provenance using trace elements in igneous zircon. Contrib. Mineral. Petrol. 170, 1–26.

Hanchar, J.M., van Westrenen, W., 2007. Rare earth element behavior in zircon-melt systems. Elements 3, 37–42.

Hanchar, J.M., Finch, R.J., Hoskin, P.W.O., Watson, E.B., Cherniak, D.J., Mariano, A.N., 2001. Rare earth elements in synthetic zircon: part 1. Synthesis, and rare earth element and phosphorus doping. Am. Mineral. 86, 667–680.

Harrison, T.M., 2009. The Hadean crust: evidence from >4 Ga zircons. Annu. Rev. Earth Planet. Sci. 37, 479–505.

Hinton, R.W., Upton, B.G.J., 1991. The chemistry of zircon: variations within and between large crystals from syenite and alkali basalt xenoliths. Geochim. Cosmochim. Acta 55, 3287–3302.

Hoaglund, S., 2010. U–Pb Geochronology of the Duluth Complex and Related Hypabyssal Intrusions: Investigating the Emplacement History of a Large Multiphase Intrusive Complex Related to the 1.1 Ga Midcontinent Rift. University of Minnesota (103 pp.). (M.Sc. thesis).

Hofmann, A.E., Valley, J.W., Watson, E.B., Cavosie, A.J., Eiler, J.M., 2009. Sub-micron scale distributions of trace elements in zircon. Contrib. Mineral. Petrol. 158, 317–335.

Hoskin, P.W., 2000. Patterns of chaos: fractal statistics and the oscillatory chemistry of zircon. Geochim. Cosmochim. Acta 64, 1905–1923.

Hoskin, P.W.O., 2005. Trace-element composition of hydrothermal zircon and the alteration of Hadean zircon from the Jack Hills, Australia. Geochim. Cosmochim. Acta 69, 637–648.

Hoskin, P.W.O., Ireland, T.R., 2000. Rare earth element chemistry of zircon and its use as a provenance indicator. Geology 28, 627–630.

Hoskin, P.W.O., Schaltegger, U., 2003. The composition of zircon and igneous and metamorphic petrogenesis. In: Hanchar, J.M., Hoskin, P.W.O. (Eds.), Zircon. Miner. Soc. Amer. Rev. Miner. Geochem. 53, pp. 27–62.

Hoskin, P.W.O., Kinny, P.D., Wyborn, D., Chappell, B.W., 2000. Identifying accessory mineral saturation during differentiation in granitoid magmas: an integrated approach. J. Petrol. 41, 1365–1396.

Ibañez-Mejia, M., Pullen, A., Arenstein, J., Gehrels, G.E., Valley, J., Ducea, M.N., Mora, A.R., Pecha, M., Ruiz, J., 2015. Unraveling crustal growth and reworking processes in complex zircons from orogenic lower-crust: the Proterozoic Putumayo Orogen of Amazonia. Precambrian Res. 267, 285–310.

Kinny, P.D., Maas, R., 2003. Lu–Hf and Sm–Nd isotope systems in zircon. Rev. Mineral. Geochem. 53, 327–341.

Long, X., Sun, M., Yuan, C., Kröner, A., Hu, A., 2012. Zircon REE patterns and geochemical characteristics of Paleoproterozoic anatectic granite in the northern Tarim Craton, NW China: implications for the reconstruction of the Columbia supercontinent. Precambrian Res. 222, 474–487.

Luo, Y., Ayers, J.C., 2009. Experimental measurements of zircon/melt trace-element partition coefficients. Geochim. Cosmochim. Acta 73, 3656–3679.

Marshall, A.S., Macdonald, R., Rogers, N.W., Fitton, J.G., Tindle, A.G., Nejbert, K., Hinton, R.W., 2009. Fractionation of peralkaline silicic magmas: the Greater Olkaria Volcanic Complex, Kenya Rift Valley. J. Petrol. 50, 323–359.

Mattinson, J.M., 2010. Analysis of the relative decay constants of ^{235}U and ^{238}U by multistep CA-TIMS measurements of closed-system natural zircon samples. Chem. Geol. 275, 186–198.

McDonough, W.F., Sun, S.S., 1995. The composition of the Earth. Chem. Geol. 120, 223–253.

Nagasawa, H., 1970. Rare earth concentrations in zircons and apatites and their host dacites and granites. Earth Plan. Sci. Lett. 9, 359–364.

Nardi, L.V.S., Formoso, M.L.L., Müller, I.F., Fontana, E., Jarvis, K., Lamarão, C., 2013. Zircon/rock partition coefficients of REEs, Y, Th, U, Nb, and Ta in granitic rocks: uses for provenance and mineral exploration purposes. Chem. Geol. 335, 1–7.

Paton, C., Woodhead, J.D., Hellstrom, J.C., Hergt, J.M., Greig, A., Maas, R., 2010. Improved laser ablation U–Pb zircon geochronology through robust downhole fractionation correction. Geochem. Geophys. Geosyst. 11.

Peck, W.H., Valley, J.W., Wilde, S.A., Graham, C.M., 2001. Oxygen isotope ratios and rare earth elements in 3.3 to 4.4 Ga zircons: ion microprobe evidence for high ^{18}O continental crust and oceans in the Early Archean. Geochim. Cosmochim. Acta 65, 4215–4229.

Profeta, L., Ducea, M.N., Chapman, J.B., Paterson, S.R., Henriquez, S.M., Kirsch, M., Petrescu, L., DeCelles, P.G., 2015. Quantifying crustal thickness over time in magmatic arcs. Sci. Report. 5.

Reid, M.R., Vazquez, J.A., Schmitt, A.K., 2011. Zircon-scale insights into the history of a Supervolcano, Bishop Tuff, Long Valley, California, with implications for the Ti-in-zircon geothermometer. Contrib. Mineral. Petrol. 161.2, 293–311.

Reiners, P.W., 2005. Zircon (U–Th)/He thermochronometry. Rev. Mineral. Geochem. 58, 151–179.

Rubatto, D., 2002. Zircon trace element geochemistry: partitioning with garnet and the link between U–Pb ages and metamorphism. Chem. Geol. 184, 123–138.

Rubatto, D., Hermann, J., 2007. Experimental zircon/melt and zircon/garnet trace element partitioning and implications for the geochronology of crustal rocks. Chem. Geol. 241, 38–61.

Rudnick, R.L., Fountain, D.M., 1995. Nature and composition of the continental crust: a lower crustal perspective. Rev. Geophys. 33, 267–309.

Sano, Y., Terada, K., Fukuoka, T., 2002. High mass resolution ion microprobe analysis of rare earth elements in silicate glass, apatite and zircon: lack of matrix dependency. Chem. Geol. 184, 217–230.

Shannon, R.D., 1976. Revised effective ionic radii and systematic studies of interatomic distances in halides and chalcogenides. Acta Crystallogr. A32, 751–767.

Taylor, R.J.M., Harley, S.L., Hinton, R.W., Elphick, S., Clark, C., Kelly, N.M., 2015. Experimental determination of REE partition coefficients between zircon, garnet and melt: a key to understanding high-T crustal processes. J. Metamorph. Geol. 33, 231–248.

Thomas, J.B., Bodnar, R.J., Shimizu, N., Sinha, A.K., 2002. Determination of zircon/melt trace element partition coefficients from SIMS analysis of melt inclusions in zircon. Geochim. Cosmochim. Acta 66, 2887–2901.

Trail, D., Mojzsis, S.J., Harrison, T.M., Schmitt, A.K., Watson, E.B., Young, E.D., 2007. Constraints on Hadean zircon protoliths from oxygen isotopes, Ti-thermometry, and rare earth elements. Geochem. Geophys. Geosyst. 8.

Trail, D., Watson, E.B., Tailby, N.D., 2012. Ce and Eu anomalies in zircon as proxies for the oxidation state of magmas. Geochim. Cosmochim. Acta 97, 70–87.

Valley, J.W., Chiarenzelli, J.R., McLelland, J.M., 1994. Oxygen isotope geochemistry of zircon. Earth Plan. Sci. Lett. 126, 187–206.

Watson, B.E., 1980. Some experimentally determined zircon/liquid partition coefficients for the rare earth elements. Geochim. Cosmochim. Acta 44, 895–897.

Watson, E.B., 1985. Henry law behavior in simple systems and in magmas—criteria for discerning concentration-dependent partition coefficients in nature. Geochim. Cosmochim. Acta 49, 917–923.

Watson, E.B., 1996. Surface enrichment and trace-element uptake during crystal growth. Geochim. Cosmochim. Acta 60, 5013–5020.

Watson, E.B., Harrison, T.M., 1983. Zircon saturation revisited: temperature and composition effects in a variety of crustal magma types. Earth Planet. Sci. Lett. 64, 295–304.

Watson, E.B., Harrison, T.M., 2005. Zircon thermometer reveals minimum melting conditions on earliest Earth. Science 308, 841–844.

Watson, E.B., Liang, Y., 1995. A simple model for sector zoning in slowly grown crystals: implications for growth rate and lattice diffusion, with emphasis on accessory minerals in crustal rocks. Am. Mineral. 80, 1179–1187.

Wedepohl, K.H., 1995. The composition of the continental crust. Geochim. Cosmochim. Acta 59, 1217–1232.

Whitehouse, M.J., Kamber, B.S., 2002. On the overabundance of light rare earth elements in terrestrial zircons and its implication for Earth's earliest magmatic differentiation. Earth Plan. Sci. Lett. 204, 333–346.

Wiedenbeck, M., Hanchar, J.M., Peck, W.H., Sylvester, P., Valley, J., et al., 2004. Further characterisation of the 91500 zircon crystal. Geostand. Geoanal. Res. 28, 9–39.

Wilde, S.A., Valley, J.W., Peck, W.H., Graham, C.M., 2001. Evidence from detrital zircons for the existence of continental crust and oceans on the Earth 4.4 Gyr ago. Nature 409, 175–178.

Wilson, C.J.N., Hildreth, W.H., 1997. The Bishop Tuff; new insights from eruptive stratigraphy. J. Geol. 105, 407–439.

Woodhead, J.D., Hellstrom, J.C., Hergt, J.M., Greig, A., Maas, R., 2007. Isotopic and elemental imaging of geological materials by laser ablation inductively coupled plasma mass spectrometry. J. Geostand. Geoanal. Res. 31, 331–343.

Yang, T.N., Zhang, H.R., Liu, Y.X., Wang, Z.L., Song, Y.C., Yang, Z.S., Tian, S.H., Xie, H.Q., Hou, K.J., 2011. Permo-Triassic arc magmatism in central Tibet: evidence from zircon U–Pb geochronology, Hf isotopes, rare earth elements, and bulk geochemistry. Chem. Geol. 284, 270–282.